



Proton-21 Electrodynamics Laboratory

**Results of experiments
on collective nuclear reactions
in superdense substance**

Kyiv
2004

CONTENTS

INTRODUCTION.....	3
DESCRIPTION OF THE EXPERIMENT.....	3
MEASUREMENT OF THE DYNAMIC PROCESS PARAMETERS.....	4
OPTICAL RADIATION INITIATED IN THE COMPRESSION ZONE	4
REGISTRATION OF FAST IONS OF THE EXPANDING PLASMA EXPANDING IN COURSE OF THE EXPLOSIVE DESTRUCTION OF THE TARGET	7
IMAGE OF THE COMPRESSION ZONE REGISTERED USING A PINHOLE CAMERA AND A FINE- MESH COLLIMATOR.....	9
COMPARISON OF THE X-RAY AND γ -RAY SPECTRA OF A QUASIPOINT SOURCE INITIATED IN THE ZONE OF ELECTRON BEAM-INDUCED COMPRESSION AND ASTROPHYSICAL OBJECTS	11
ANALYTICAL STUDY	12
ANALYSIS OF THE ELEMENT COMPOSITION OF SAMPLES AFTER EXPERIMENT	13
<i>Local analysis of the accumulating screens by X-ray electron probe microanalysis</i>	<i>18</i>
<i>Integral analysis of the accumulating screens by glow-discharge mass-spectrometry ..</i>	<i>18</i>
ANALYSIS OF THE ISOTOPE COMPOSITION OF INERT GASES IN A RESIDUAL ATMOSPHERE OF THE VACUUM CHAMBER.....	19
ANALYSIS OF THE ISOTOPE COMPOSITION OF ACCUMULATING SCREENS.....	20
DISTRIBUTIONS OF VARIOUS CHEMICAL ELEMENTS OVER DEPTH IN ACCUMULATING SCREENS	21
DECREASE IN THE γ-ACTIVITY OF RADIOACTIVE ISOTOPE OF COBALT ⁶⁰CO	22
EXTRAORDINARY RESULTS	23
REGISTRATION OF THE UNIDENTIFIABLE ATOMIC MASSES WITH THE MASS NUMBER >220 A.M.U IN NEAR-SURFACE LAYERS OF ACCUMULATING SCREENS BY THE SECONDARY ION MASS-SPECTROMETRY	23
REGISTRATION OF THE SCATTERING CENTERS, CORRESPONDING TO THE MASS NUMBERS > 200 A.M.U., IN THE ENERGY SPECTRA OF SCATTERED α -PARTICLES AND NITROGEN IONS (¹⁴ N).....	23
REGISTRATION OF THE UNIDENTIFIABLE PEAKS OF CHARACTERISTIC X-RAY AND AUGER EMISSION IN THE ELEMENTAL COMPOSITION ANALYSIS OF THE ACCUMULATING SCREENS SURFACE.....	24
STUDY OF THE SAMPLES BY INDEPENDENT LABORATORIES	25
EXTRACTS FROM THE OFFICIAL CONCLUSION OF THE CONCERN “LUCH”, RUSSIA, CONCERNING THE ANALYZED OBJECTS GIVEN BY THE FIRM “PROTON-21” FOR MASS SPECTROMETRIC ANALYSIS ON A DEVICE “FINNIGAN” MAT-262:.....	25
EXTRACTS FROM THE OFFICIAL CONCLUSION OF MICRO PHOTONICS (SURFACE TEST), REPORT SIMS-030623 FOR UNITED METALS LLC (USA):	25
RESULTS AND CONCLUSIONS	26

Introduction

In this report, we present the results of experiments on collective nuclear reactions in superdense substance. The experiments were carried out at the Proton-21 Electrodynamics Research Laboratory (Kyiv, Ukraine) in 1999–2004 (Dr. S. V. Adamenko is the chief researcher of the project, and Dr. A. G. Kokhno is the company's general director) with the purpose of developing a fundamentally new technology for utilization of radioactive wastes.

The research is based on the idea of initiation of a self-focusing cumulative process of shock compression of target substance to superhigh densities, with possible nuclear transmutation of the substance whereby radioactive isotopes are transformed into stable ones.

Description of the experiment

The above-mentioned idea was realized in an experimental setup able to transfer up to 1 kJ of energy to a solid target (Figs. 1a, 13) within the impulse duration of the order of 10^{-8} sec. In this case, the power density in the compression area reaches the level of 10^{22} W·cm⁻³. The experiments were carried out in vacuum of about 10^{-3} Pa.

Prior to working with radioactive targets, we worked on the process technology and optimal parameters of the experimental setup using for targets and accumulating screens (Fig. 1, 18) chemically pure copper (Cu with purity of 99.99%), silver (Ag with purity of 99.99%), tantalum (Ta with purity of 99.68%), lead (Pb with purity of 99.91%), and other materials.

The experiments performed in that setup have shown that a target, into which energy is entered from outside, is destroyed by the explosion from inside (Figs. 1b, 14). The explosion leads to a radial dispersion of the target substance, which is then precipitated on a special accumulating screen which has the form of a disk (Figs. 1, 18). The precipitated items have the form of irregularly distributed drops, balls, films, etc.

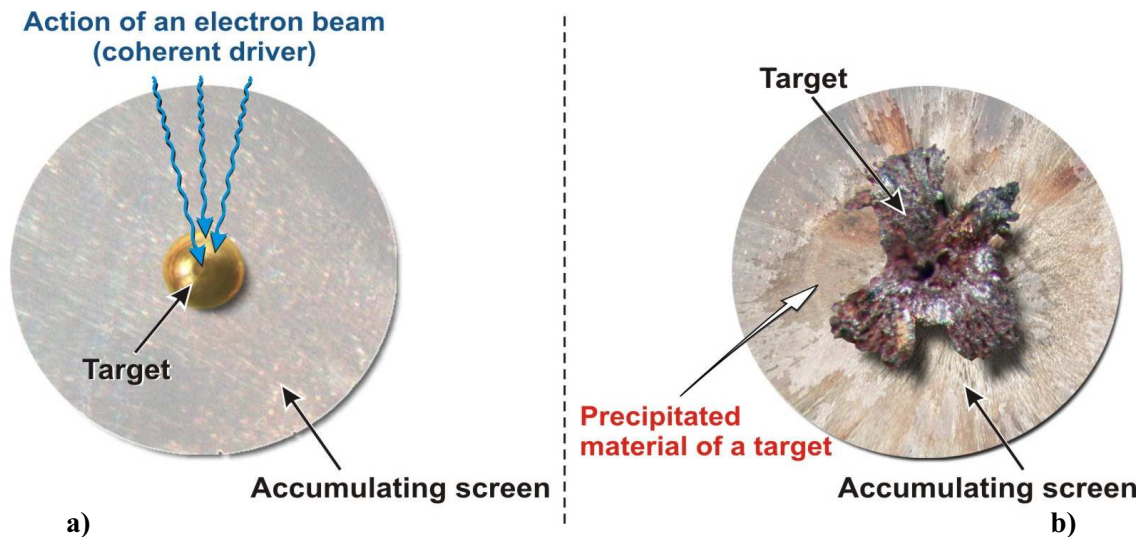


Fig. 1. Scheme of the experiment on target material compression that depicts the initial state of the sample (a) and its state after the experiment (b).

Measurement of the dynamic process parameters

Optical radiation initiated in the compression zone

Optical radiation of the plasma around the compression zone was registered by the SL 40-2-3648 USB spectrometer. It is a CCD-based two-channel system for optical spectrum registration. Dispersing element in each channel of the spectrometer is a diffraction grating with the following parameters:

- dimensions of 12×10 mm,
- 600 slits per 1 mm,
- reverse linear dispersion: 35.09 nm/mm in the first channel, and 31.95 nm/mm in the second channel,
- wavelength resolution: less than 1.5 nm.

Registration was performed through the output acrylic glass window 4 mm thick. Receiver of the light signal was located at the distance of about 6 m from the compression area, and connected by paired 2-m long optical fiber to the spectrometer and FEU-30 fast photoelectric multiplier.

Signal from the photoelectric multiplier was registered with a digital oscillograph. Thus, the optical spectrum and duration of the light flash were registered simultaneously. The spectrometer was calibrated as follows:

- in the near ultraviolet range – using continuous spectrum of the DDS-80 deuterium lamp with the nameplate luminous energy intensity of about 1.8 mW/stere in the spectral range of 215...300 nm;
 - in the visible light range – using continuous spectrum of the incandescent 100-W lamp.
- Calibration in the optical range was checked using individual copper lines with known intensity.

A typical spectrum of the optical radiation of the plasma bunch in the shock compression area of the target is presented in Fig. 2.

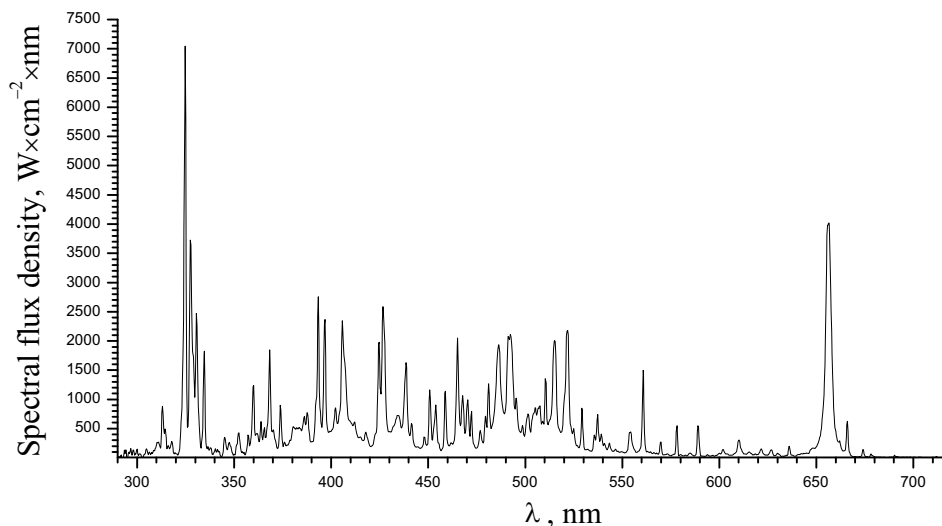


Fig. 2. Optical radiation spectrum of the plasma bunch in the experiment No. 3981.

Optical spectra were processed using Peak Fit standard software. It can handle line spectra consisting of up to one hundred spectral lines.

Estimation of the plasma bunch parameters in the typical experiment No. 3981

1) Ion component (Table 1)

- a) Average energy and velocity of ions are 9.48 keV and 1.6×10^7 cm·sec⁻¹, respectively, calculated according Doppler broadening formulas.
- b) Number of radiating atoms is 8.03×10^{17} , calculated from the growth graphs of integral absorption for spectral lines (“growth curves”). The intensity of individual spectral lines was normalized by the effective cross-section of the plasma bunch and radiation duration.
- c) Ion component energy is about 750.89 J, calculated based on the analysis of Gaussian component in spectral lines of different chemical elements’ individual ions.

2) Electron component

- a) Electron temperature is $T_e \cong 0.36$ keV, estimated from amplitudes of hydrogen lines.
- b) Electron density is about 1.2×10^{17} cm⁻³ (shock approximation), calculated from Lorentz components of spectral lines, assuming that the lines broadening is caused by ion-electron collisions.
- c) Total number of electrons in the volume of the plasma bunch is $N_e \approx 1 \times 10^{18}$.
- d) Electron component energy is about 60 J.

The effective size of the plasma bunch is 3 cm (diameter), calculated from the effective duration of radiation and average ion velocity. Effective duration of radiation was assumed to be the duration of the light flash registered with the photoelectric multiplier ($\tau = 60$ ns in the experiment No. 3981).

It should be noted that in the plasma bunch spectrum spectral lines of ions of Fe, Ni, and other chemical elements are present (see Table 1). Those elements were not present in the initial composition of the target material; nevertheless, in terms of the energy and numbers of emitting atoms, they are competing with the basic elements of that material (Pb, Cu).

Comparison of the radiation parameters of the experiment No. 3981 with those of the experiment that was performed in the imitation mode* shows significant differences in the corpuscular component of the plasma, though optical spectra seems to be similar and value of the light output are close (14 J and 9 J, respectively). The total output of the corpuscular energy in the experiment No. 3981 is about 808 J, which is by two orders higher than that of the imitation mode (about 12 J).

* The imitation mode has the same energy parameters of the initial impact, but does not initiate the cumulative process of energy self-concentration in the target.

Table 1. Estimated energy output of the ion component of plasma bunch near the compression area, taking into account the stages of ionization (Experiment No. 3981, target – Pb, Cu)

Chemical element	Average ion energy, keV	Average ion velocity, cm·sec ⁻¹	Number of radiating atoms	Total energy of ions, J
H	1.6E-01 ±3.8E-02	1.7E+07 ±2.2E+06	1.72E+17	5.46
C	1.5E+00 ±2.2E-01	1.5E+07 ±1.1E+06	3.21E+16	8.90
F	1.2E+00 ±5.9E-02	1.1E+07 ±2.8E+05	2.04E+17	14.40
Al	3.9E+00 ±5.1E-01	1.5E+07 ±1.1E+06	4.19E+15	2.69
Cl	5.7E+00 ±6.3E-01	1.7E+07 ±7.5E+05	6.72E+15	6.60
Ca	6.1E+00 ±9.2E-01	1.7E+07 ±1.3E+06	6.61E+15	4.96
Ti	9.4E+00 ±5.0E-01	1.9E+07 ±4.0E+05	2.00E+16	31.00
Cr	8.9E+00 ±1.6E+00	1.8E+07 ±1.6E+06	5.14E+15	6.73
Fe	7.7E+00 ±5.1E-01	1.6E+07 ±5.3E+05	1.33E+17	139.00
Ni	9.1E+00 ±9.5E-01	1.6E+07 ±9.9E+05	7.53E+16	127.00
Cu	9.0E+00 ±1.0E+00	1.6E+07 ±9.1E+05	7.52E+16	138.00
Zn	1.1E+01 ±1.3E+00	1.8E+07 ±1.2E+06	1.98E+16	41.50
Mo	1.4E+01 ±1.2E+00	1.6E+07 ±7.5E+05	1.04E+16	22.80
Xe	1.8E+01 ±5.5E+00	1.6E+07 ±2.2E+06	1.78E+15	6.28
Ba	1.7E+01 ±6.9E+00	1.5E+07 ±2.8E+06	2.15E+15	8.57
Pb	2.9E+01 ±3.4E+00	1.6E+07 ±9.4E+05	3.51E+16	187.00
TOTAL			8.03E+17	750.89

Table 2. Estimated energy output of the ion component of plasma bunch near the compression area, taking into account the stages of ionization (experiment in the imitation mode)

Chemical element	Average ion energy, keV	Average ion velocity, cm·sec ⁻¹	Number of radiating atoms	Total energy of ions, J
H	5.2E-03 ±8.5E-04	3.1E+06 ±2.7E+05	1.78E+16	0.02
C	6.5E-02 ±6.2E-03	3.2E+06 ±1.5E+05	7.83E+15	0.08
O	1.0E-01 ±4.5E-03	3.5E+06 ±7.8E+04	1.55E+16	0.24
Cl	2.4E-01 ±1.2E-02	3.6E+06 ±8.9E+04	2.82E+15	0.10
Ca	2.9E-01 ±5.2E-02	3.5E+06 ±1.8E+05	1.35E+15	0.06
Ti	3.4E-01 ±2.9E-02	3.7E+06 ±1.6E+05	2.82E+15	0.14
Cr	3.9E-01 ±4.0E-02	3.8E+06 ±1.9E+05	1.23E+15	0.09
Fe	3.9E-01 ±2.6E-02	3.6E+06 ±1.2E+05	3.17E+15	0.17
Ni	4.8E-01 ±4.6E-02	4.0E+06 ±1.9E+05	1.94E+15	0.13
Cu	4.6E-01 ±2.0E-02	3.7E+06 ±8.3E+04	9.44E+16	5.88
Zn	4.1E-01 ±3.8E-02	3.5E+06 ±1.6E+05	4.58E+15	0.32
Mo	7.3E-01 ±1.1E-01	3.8E+06 ±2.8E+05	2.96E+15	0.31
Pb	1.1E+00 ±1.7E-01	3.2E+06 ±2.5E+05	1.62E+15	0.31
TOTAL			1.58E+17	7.83

Registration of fast ions of the expanding plasma expanding in course of the explosive destruction of the target

To register fast ions, we used the following:

- CR-39 track detectors CR-39 allowing one to see the cumulative effect of the impact of ion streams on the ion receivers for various configurations of ion optical devices;
- magnetic analyzers, which enable one to analyze the oscillograms of electric signals from ions, and to measure the time-of-flight parameters in every experiment.

The track detectors, which were placed directly in the radiation field of the plasma front at a distance of 3...13 cm from the shock compression center, demonstrate the complete filling by “plasma-produced tracks” (Fig. 3).

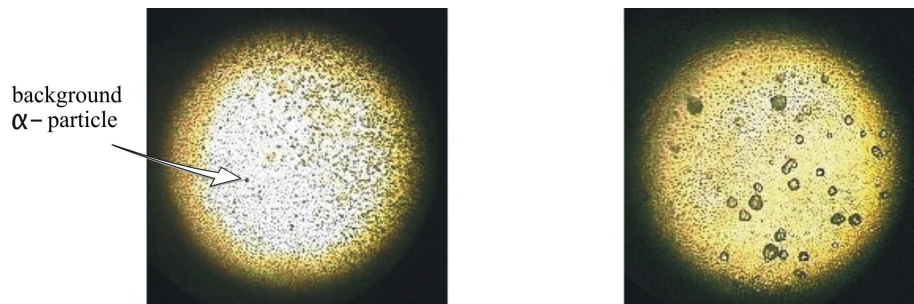


Fig. 3. Pattern of the detector filling with tracks, showing both small (plasma-produced) and pronounced large tracks of ion jets (a), tracks of particularly large plasma particles (b).

The density of plasma tracks registered at distances of about 10 cm from the center of the shock compression area reaches the levels of $10^8/\text{cm}^2$ or more, with absolute packing of tracks, virtually isotropic for weak micrometer-scale tracks looking like etching pits. These tracks are mostly formed by ions of the target material with energies near to the track formation threshold of 10 keV/nucleon. The lower estimate for the total number of track-forming particles is $10^{10} \dots 10^{12}$. Detailed track analysis of the composition of plasma particles streams has been hindered by the lack of a complete set of calibration data.

In a number of experiments, in addition to the complete filling with plasma-produced tracks, we observed an increased number of nuclear tracks that were close or identical to those of α -particles (Fig. 4).

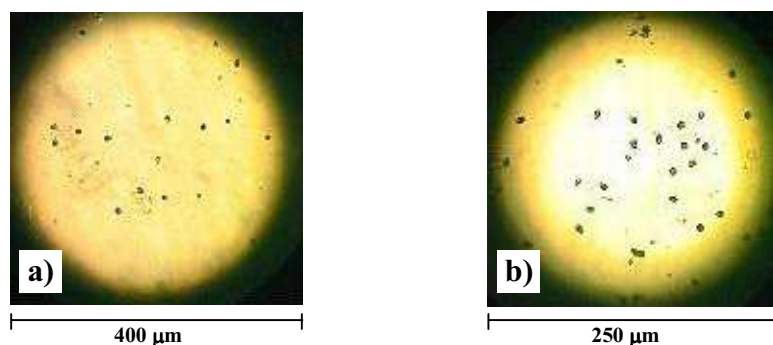


Fig. 4. Pattern of the detector filling with α -particles' tracks after it has been exposed in three experiments No. 5092, 5095, 5096 (a), and after it has been exposed for 30 seconds exposition to the ^{239}Pu source with the intensity of 10^4 impulses/min (b).

Rarely, collective centralized tracks occur, which cannot be referred to independent α -particles. As an example, in the detector located directly behind the shielding grid, a unique centralized cluster was found consisting of 276 tracks (Fig. 5).

We call reader's attention to the downward trend of inclined tracks (Fig. 5), which indicates the presence of the common momentum for this registered family of particles on the preservation of the well-pronounced centrality of the dispersion.

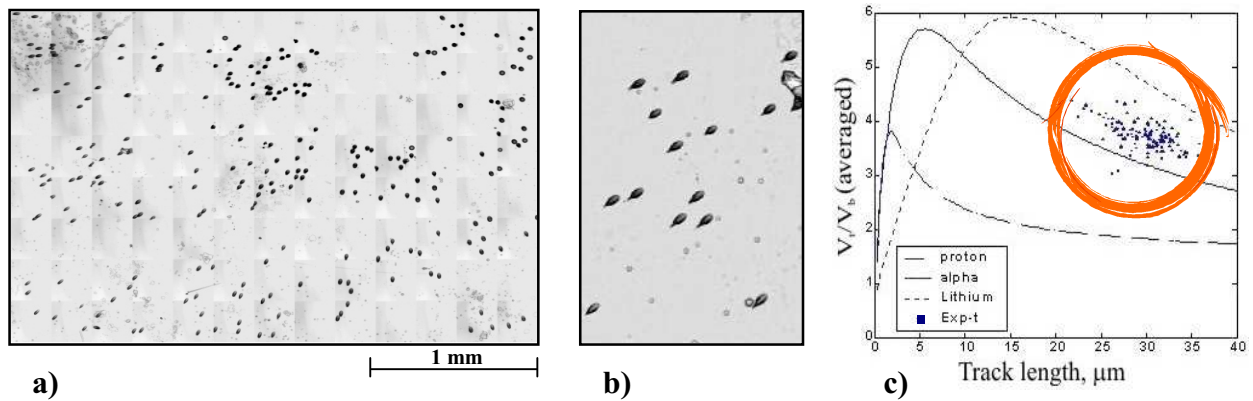


Fig. 5. The pattern of the filling of detectors by tracks including the image of centralized tracks (experiment No. 4109), the “giant” cluster of tracks composed of 276 tracks (a); an individual fragment 240×300 μm (b), the ratio of measured rates of track etching and bulk etching vs the track length (c).

The analysis of inclined tracks, which was performed by the algorithm using the results of optical measurements of tracks on a scanning optical microscope Olympus, allowed us to conclude that the cluster was composed of α -particles with energies in the range of 4...6 MeV.

On the registration of radial components of the ion flux with a magnetic analyzer situated directly in the discharge chamber, of the most interest were the measurements of electric signals of a straight-flight collector registering the fastest particles.

The measurements of electric signals showed that the fastest ions defining the current of ions in the radial direction possess the energy of about tens of keV per nucleon. We note that the determination of the total number of fast particles on the basis of the measurement of currents is hampered by influence of the electromagnetic interference on the leading edge of an early collector signal. The recalculation of the current of bunches of these ions for the “ 4π ” geometry gave the estimate which is higher by many orders as compared to 10^{12} which follows from the data on tracks.

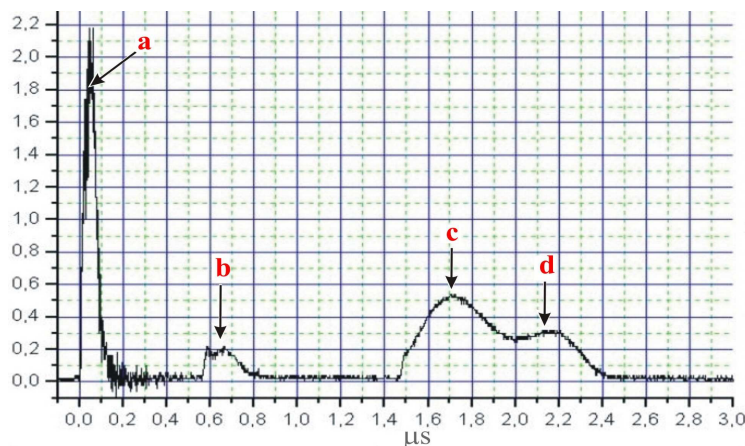


Fig. 6. The oscillogram obtained by the time-of-flight method characterizes the particle flux (current signals) of the expanding plasma of the fractured target as a function of time, light low-charge or heavy highly charged ions (a); the energy of the fastest particles, i.e. those with slightly deflected trajectories, is about 20 keV/nucleon, which is confirmed by the presence of plasma-produced tracks on the track detector in the “right through” position, heavy single-charged ions including superheavy ones or low-charge atomic clusters (b) and (c), superheavy atomic ions or atomic clusters (d).

Image of the compression zone registered using a pinhole camera and a fine-mesh collimator

The image of the plasma flash in the collapse zone is represented, as a rule, by vague objects several millimeters long, which consist of one-type plasma tracks. According to the calibration data obtained on accelerators of nuclear particles the most contrast track images are formed by the ions with energy about 100...400 keV/nucleon. The tracks of accelerated protons and deuterons with energy up to 1.6 MeV were also registered.

An example of the detector filled with tracks that were obtained by a direct projection in the pinhole camera with a small diaphragm (Fig. 7a) is shown in Fig. 7b. In Fig. 8 enlarged fragments of the image are presented, containing the tracks of 1-MeV protons and deuterons.

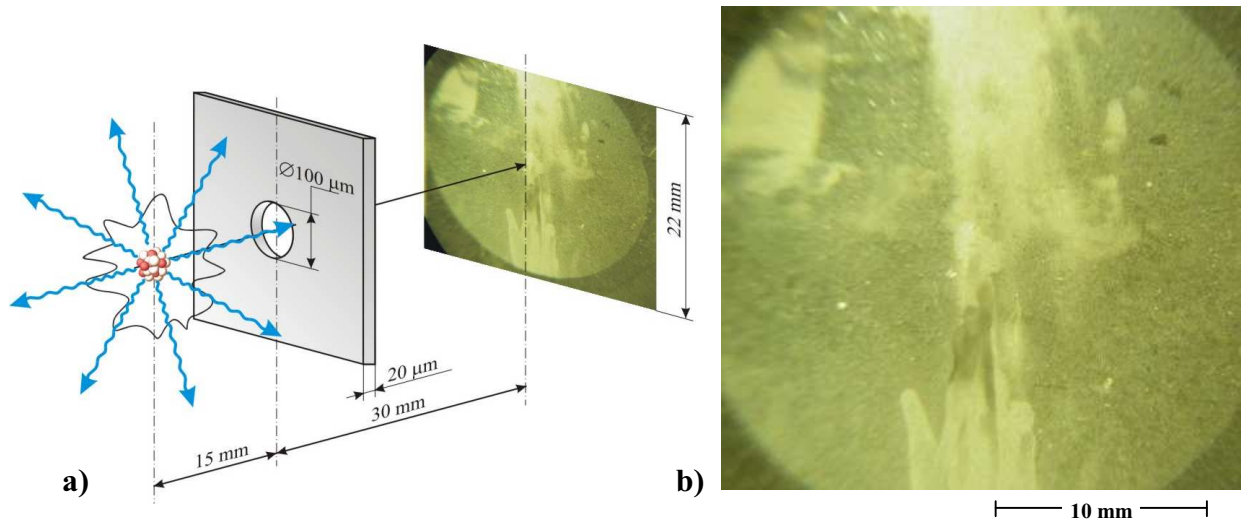


Fig. 7. Scheme of the pinhole camera taking the image of the plasma flash in the collapse zone (a); image of the detector filled with tracks in the experiment No. 5872 (b).

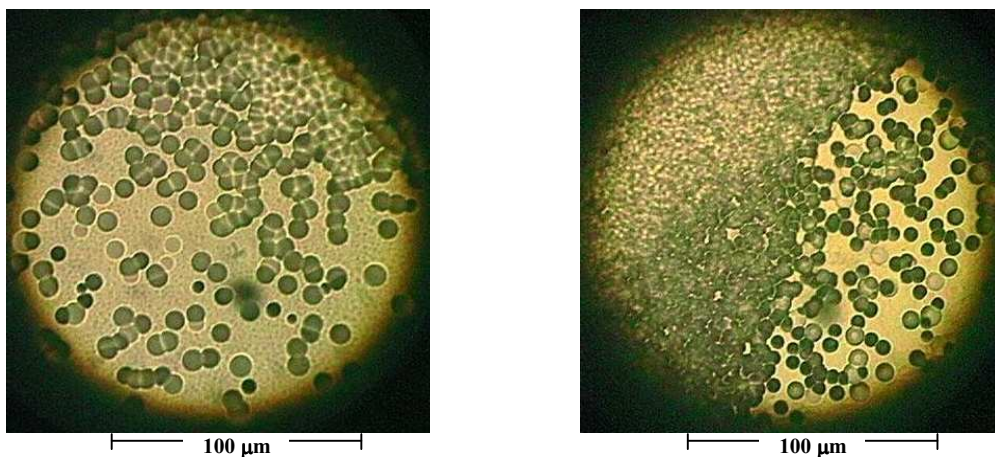


Fig. 8. Fragments of the image of the detector filled with tracks of 1-MeV protons and deuterons in the experiment No. 5872.

Comparison of the images derived in experiments with the help of fine-mesh collimator (Fig. 10) and by computer simulation (Fig. 11) leads to the following conclusions:

1. the source size is at most 200 μm ;
2. the source can have the elongated form with size in the direction of elongation up to 500 μm . In this case, the assumed transverse sizes remain to be previous;
3. for an elongated source, one can observe a considerable (varying by at least one order) inhomogeneity of the emission intensity along the source length.
4. the maximum of the spectrum of X-ray quanta is near 30–40 keV;
5. the number of X-ray quanta radially outgoing (4π) from the center of a quasipoint source is about 10^{15} during 10^{-8} sec;

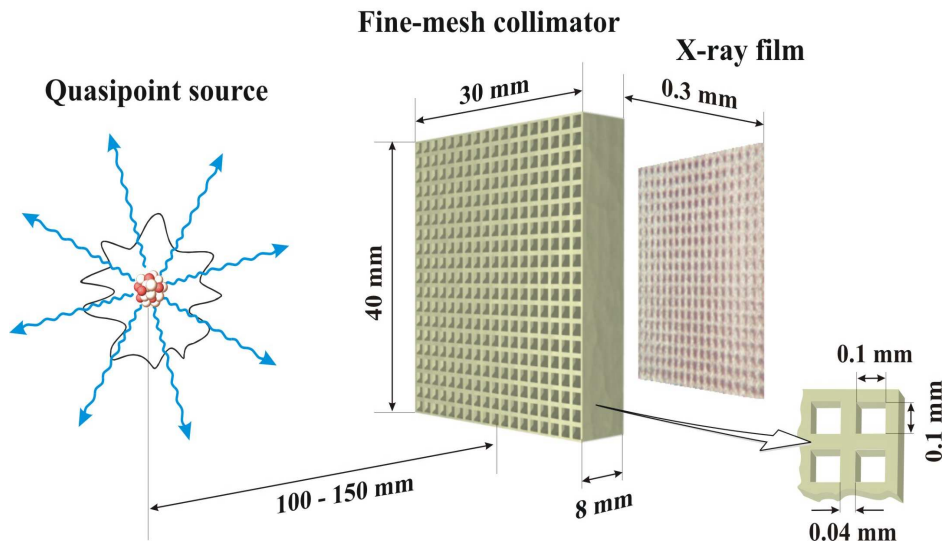


Fig. 9. Scheme of the fine-mesh collimator setup.

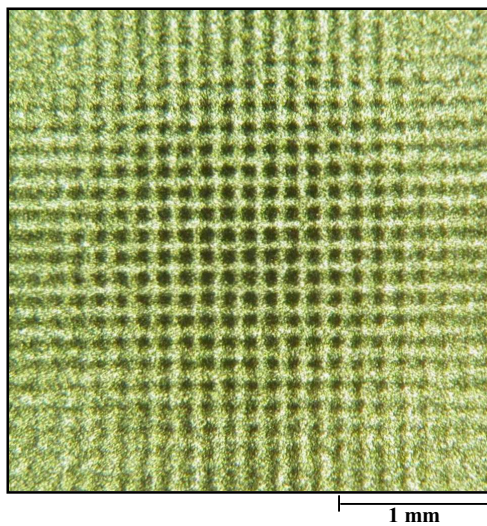


Fig. 10. Image of a quasipoint source on an X-ray film derived with the help of a fine-mesh collimator

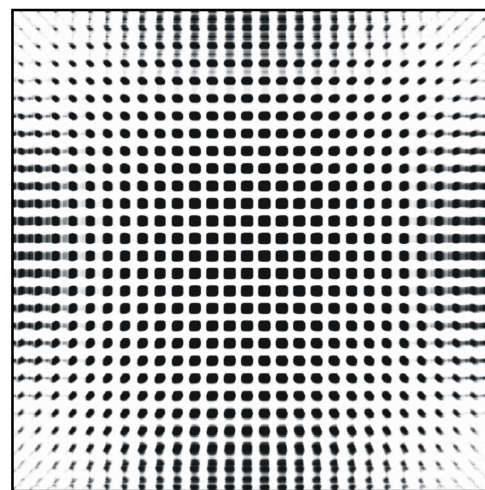


Fig. 11. Computer simulation of the passage of X-ray quanta through a fine-mesh collimator

Comparison of the X-ray and γ -ray spectra of a quasipoint source initiated in the zone of electron beam-induced compression and astrophysical objects

The spectra of astrophysical objects, such as Sun, Crab nebula pulsar, quasar 3C 273, supernova CH1987A, and short gamma-bursts, in the X-ray and γ -ranges are separated from their full emission spectra and are given on the scale convenient for the comparison with the spectrum of the quasipoint source (Fig. 12). Spectral radiant intensity of the quasipoint source is an average over 2500 experiments. As a measure of comparison the correlation coefficient was used (see Table 3).

In some experiments, the spectra of X-ray emission were derived from the filtration curves measured by GaAs detectors with the collection of copper filters from 20 mm to 11 mm in thickness. The registration of current signals from the detectors was realized by fast oscillographs “Tektronix” without preliminary amplification in the azimuth plane at a distance of 23 cm from the axis of the setup through a window made of Al of 350 mm in thickness.

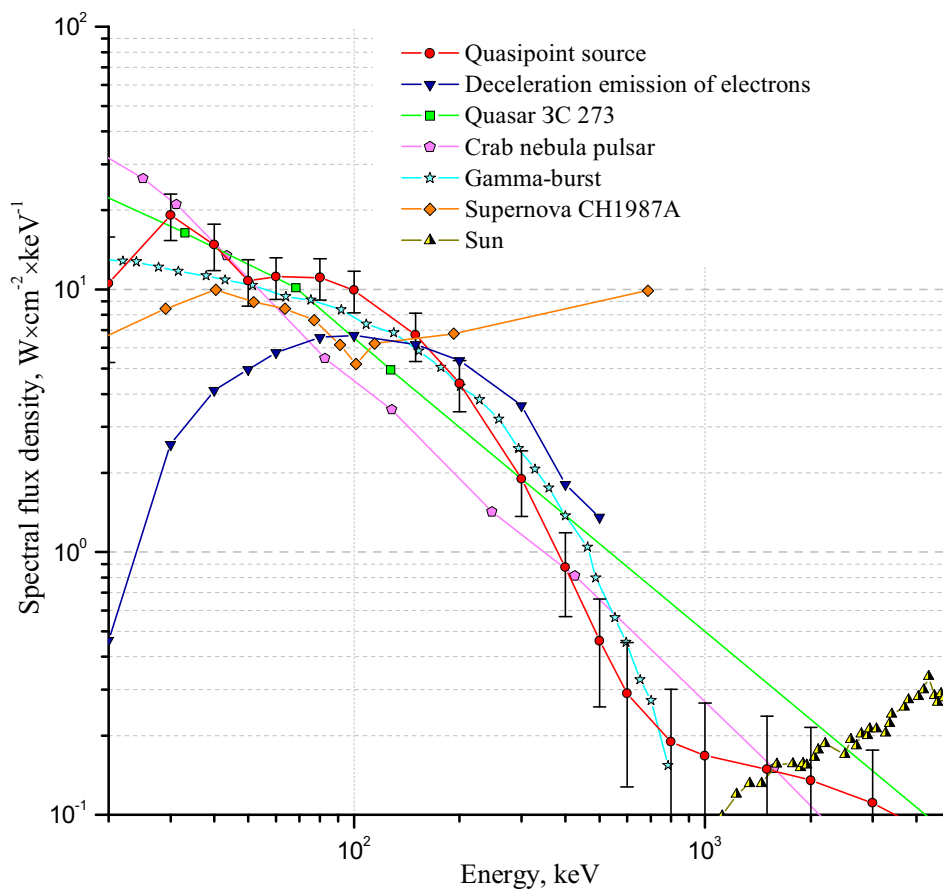


Fig. 12. Distribution of spectral radiant intensity of the quasipoint source and astrophysical objects. Logarithmic scale, for quasar 3C 273, Crab nebula pulsar, quasar 3C 273, gamma-burst, supernova CH1987A, and Sun the multipliers are 3×10^{19} , 3×10^{18} , 2×10^{17} , 2×10^{19} and 1×10^3 , respectively.

Table 3. Comparison of spectral radiant intensity of quasipoint source and some astrophysical objects.

Object	Energy range, keV	Correlation coefficients
Quasar 3C273	10...4000	0.94
Crab nebula pulsar	10...4000	0.92
Gamma-burst	20...800	0.99
Supernova CH1987A	10...700	-0.23
Sun	200...5000	-0.96
Deceleration emission	20...500	0.24

The comparison revealed that the parameters of the quasipoint source radiation in the energy range from 10 keV up to 3...5 MeV are very similar to the ones of nonstationary astrophysical objects (quasar, pulsar, gamma-bursts), that have a compact radiation area (even in the cosmic scale) and significant magnetic fields. It is worth noting that functional relations describing the continuous spectra of gamma-bursts (spectral radiant intensity $dN/dE \sim E^{-\alpha} \cdot \exp(-E/E_0)$ with $\alpha = 0.5...1.5$ and characteristic energy E_0 that is a measure of a radiation temperature and significantly changes in time in the range of 100...1000 keV) and experimental spectra of quasipoint source ($\alpha = 1$ and E_0 of several thousand keV in maximum) are equal.

The differences of quasipoint source and CH1987A spectra are mainly in the high-energy part, where the strong deficiency of photons for the quasipoint source is observed.

The spectral composition of the quasipoint source radiation differs from the one of the deceleration emission in the simulation mode experiment by high output of photons in the low-energy part of the spectrum and also by output of the photons in the high-energy part.

Analytical study

One of the problems of the performed series of experiments consisted in the derivation of an answer to the question: Do any nuclear transformations of a target material occur in the process of electron beam-induced compression? To this end, we carried out, in particular:

1. Comparison of the element composition of the initial materials of a target and an accumulating screen prior to the experiment with that of the formed condensate in order:
 - a) to discover the chemical elements in the condensate which were absent in the starting materials;
 - b) to determine the degree of increase in the concentrations of the impurity elements in the samples under study as compared to those in the initial materials.
2. Measurement of the isotope composition of chemical elements in the condensate and gases (in the working chamber volume).
3. Measurement (before and after the experiment) of the level of radioactivity of targets containing the atoms of unstable isotopes dispersed in the target volume (the method of "tagged atoms").

Analysis of the element composition of samples after experiment

From 1999 till 2004 more than 6000 dynamic compressions of solid targets were performed leading to specific explosions and the radial dispersion of a transformed target material from the collapse zone. Altogether 15000 analyzes of about 800 samples were performed and registered. The summary of the analytical methods and number of analyzes are listed in Table 4.

The analysis was performed with the use of modern methods and facilities (Table 5).

Table 4. List of analytical methods and number of analyzes

Method	Samples	Analyzes
X-ray electron probe microanalysis	698	12009
Auger-electron spectroscopy	105	1607
Mass-spectrometry	167	1631
Rutherford backscattering	51	51
TOTAL:	-----	15298

Table 5. Analytic methods and facilities used in the investigations of the element and isotope compositions of surface and near-surface layers of targets and accumulating screens

Method	Device (firm, country)
X-ray electron probe microanalysis	SX50 (CAMECA, France)
	REMMA102(Selmi, Ukraine)
	BS340 (TESLA, Czech Republic)
	Superprobe 733 (JEOL, Japan)
X-ray fluorescence analysis	RFA (KNU, Ukraine)
Auger-electron spectroscopy	JAMP-10S (JEOL, Japan)
Glow-discharge mass-spectrometry	VG 9000 (VG Elemental, UK)
Mass spectrometry of secondary post-ionized neutral particles	INA-3 (Germany)
Secondary-ion mass-spectrometry	IMS-4f (CAMECA, France)
Thermal-ionization mass-spectrometry	Finnigan MAT-262 (ThermoFinnigan, Germany)
Laser mass-spectrometry	Laser mass spectrometer (KNU, Ukraine)
Rutherford backscattering	Cyclotron ion accelerator U-120 (INR, Ukraine), Electrostatic accelerator EGP-10T ("TANDEM", INR, Ukraine)

Below, we present the photos (Figs. 14–17, 19) of metallic targets after the electron beam-induced compression experiments, and accumulating screens as well as the results of analysis of the element composition of condensed "ejections" of a substance from the zone of electron beam-induced compression. In the windows-inserts, the concentrations (in wt. %) of chemical elements in the vicinity of relevant points of the analyzed surface are given. The elements that were absent in the composition of the initial materials are highlighted.

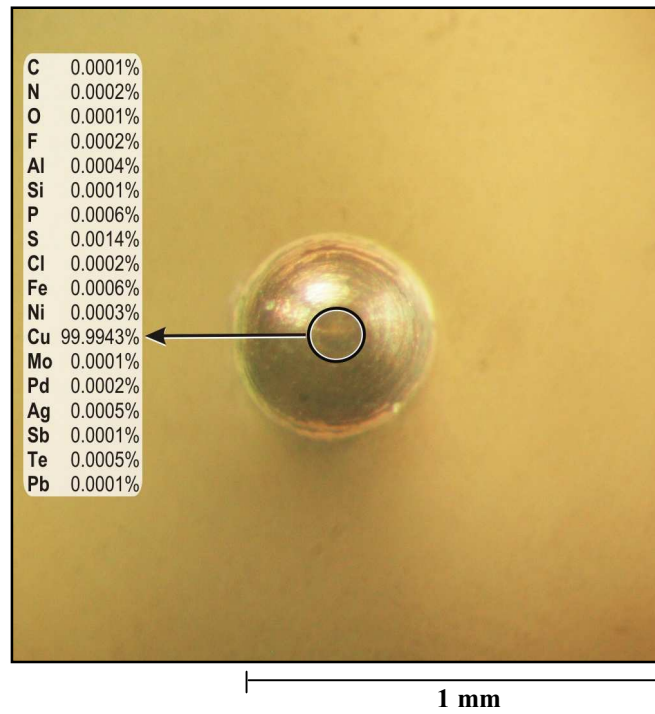


Fig. 13. The target is shown prior to the experiment.
 Material of the target is copper (Cu 99.99%).
 The method of investigation is glow-discharge mass-spectrometry.
 (VG-9000, analyzed mass range – up to 250).

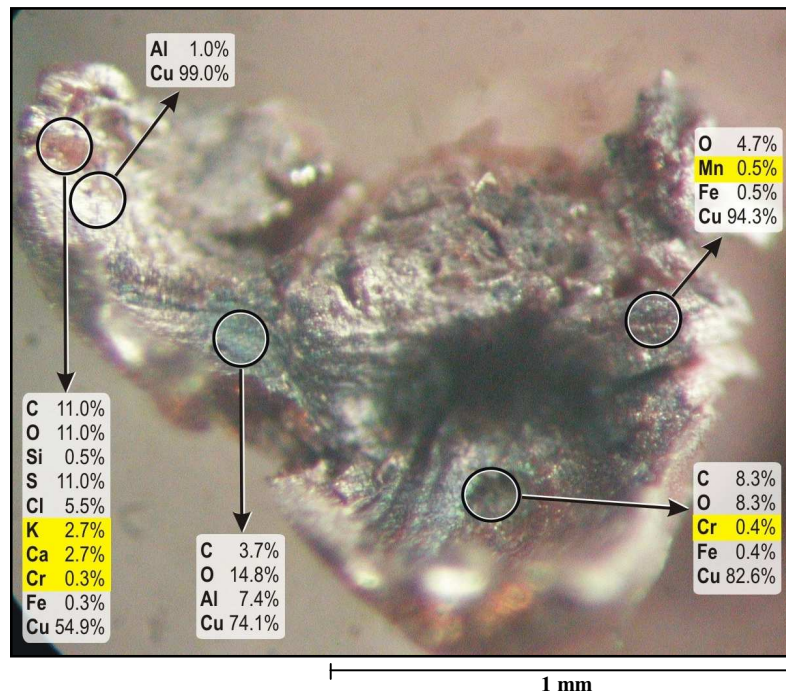


Fig. 14. Target after Experiment No. 1684.
 Material of the target is copper (Cu 99.99%).
 The method of investigation is X-ray electron probe microanalysis.
 (Element detection range – from B to U).

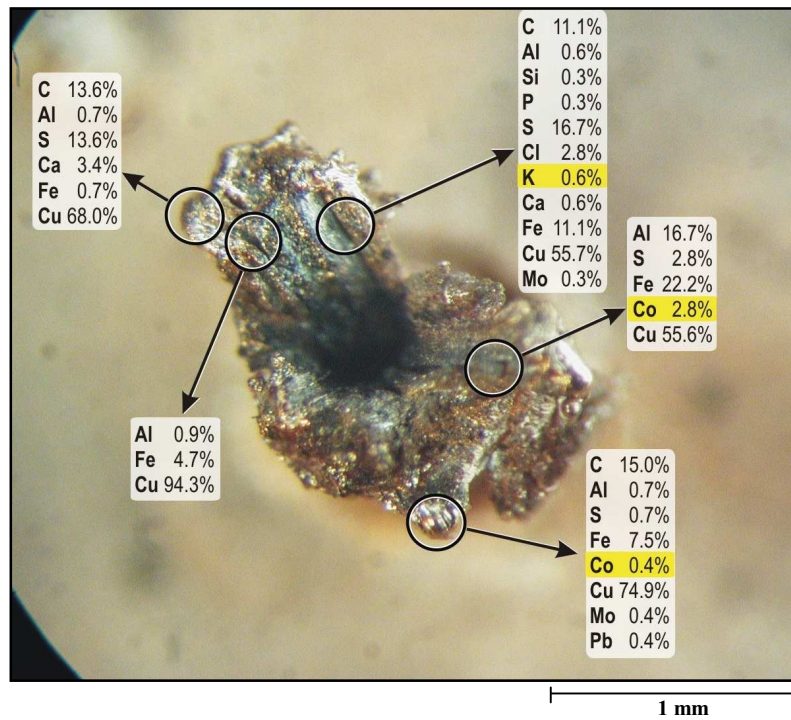


Fig. 15. Target after experiment No. 1685.
 Material of the target is copper (Cu 99.99%).
 The method of investigation is X-ray electron probe microanalysis.
 (Element detection range – from B to U).

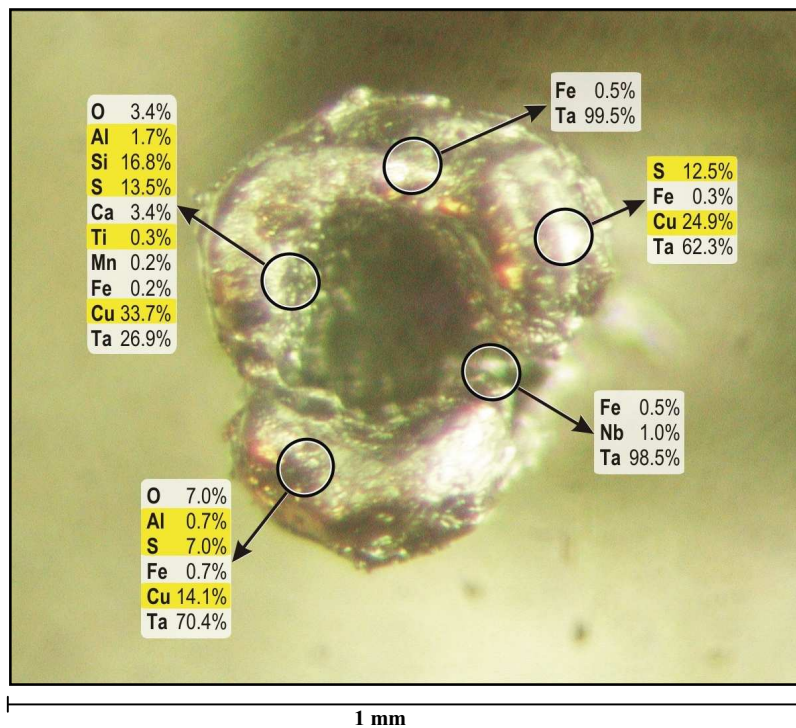


Fig. 16. Target after experiment No. 1754.
 Material of the target is tantalum (Ta 99.68%).
 The method of investigation is X-ray electron probe microanalysis.
 (Element detection range – from B to U).

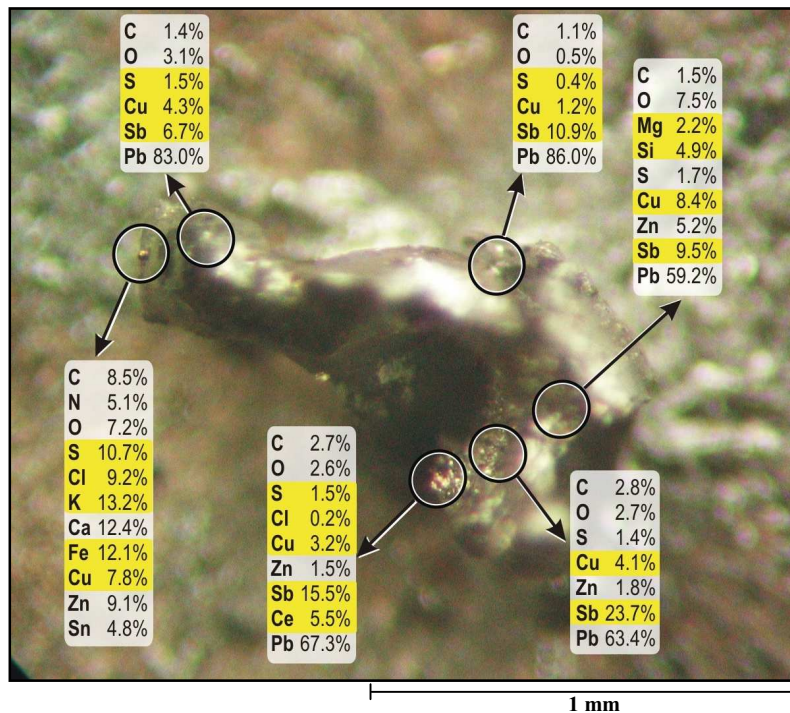


Fig. 17. Target after experiment No. 2275.
 Material of the target is lead (Pb 99.91%).
 The method of investigation is Auger-electron spectroscopy.
 (Element detection range – from Li to U)

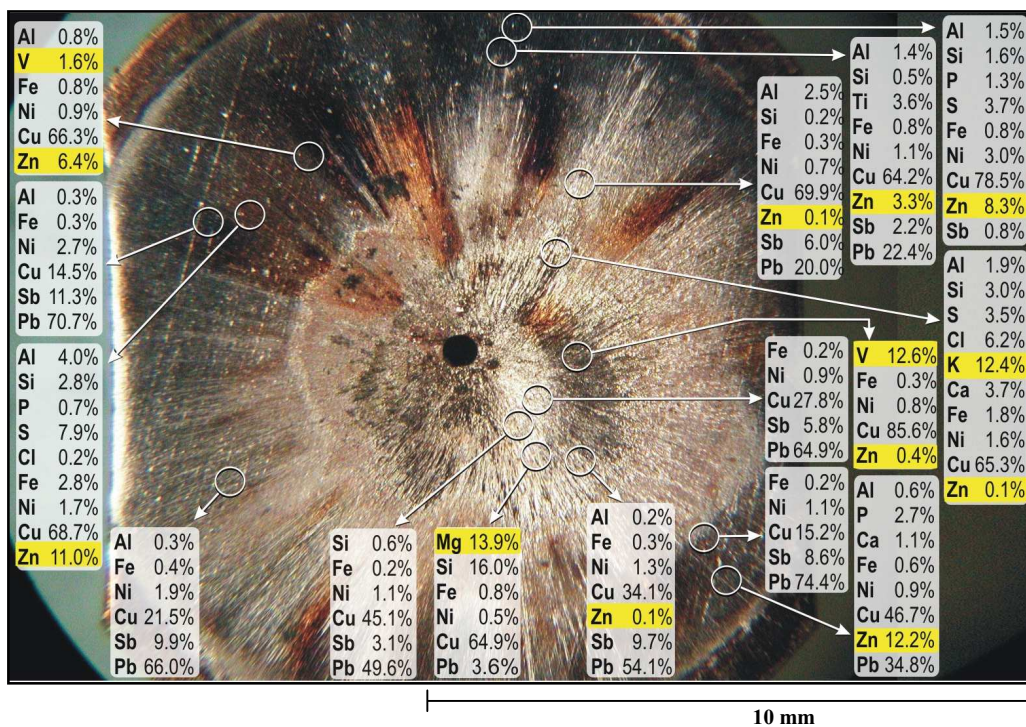


Fig. 18. Accumulating screen after experiment No. 3082.
 The material of both the accumulating screen and target is copper (Cu 99.99%).
 The method of investigation is X-ray electron probe microanalysis.
 (Element detection range – from Na to U).

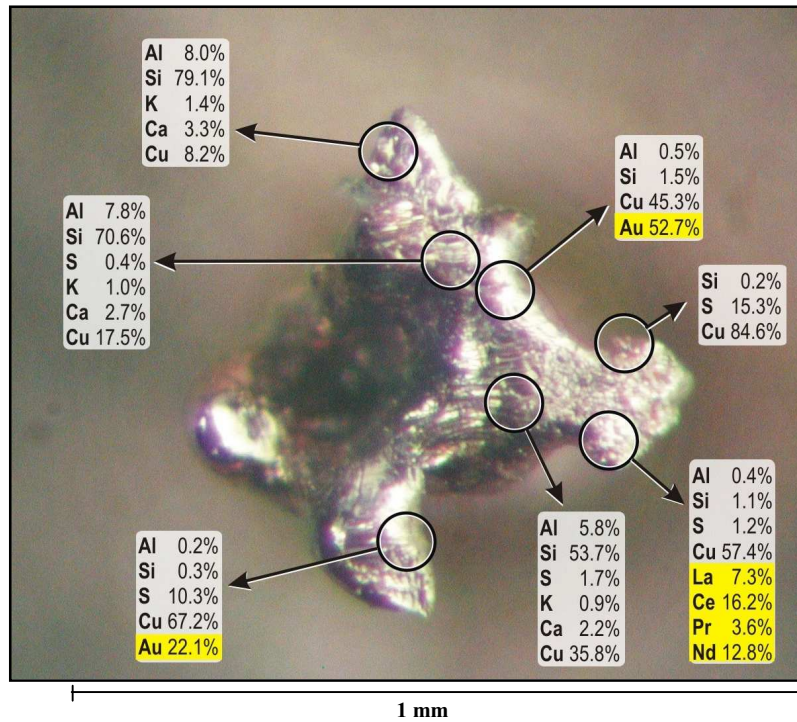


Fig. 19. Target after experiment No. 2107.
 Material of the target is copper (Cu 99.99%).
 The method of investigation is X-ray electron probe microanalysis.
 (Element detection range – from Na to U).

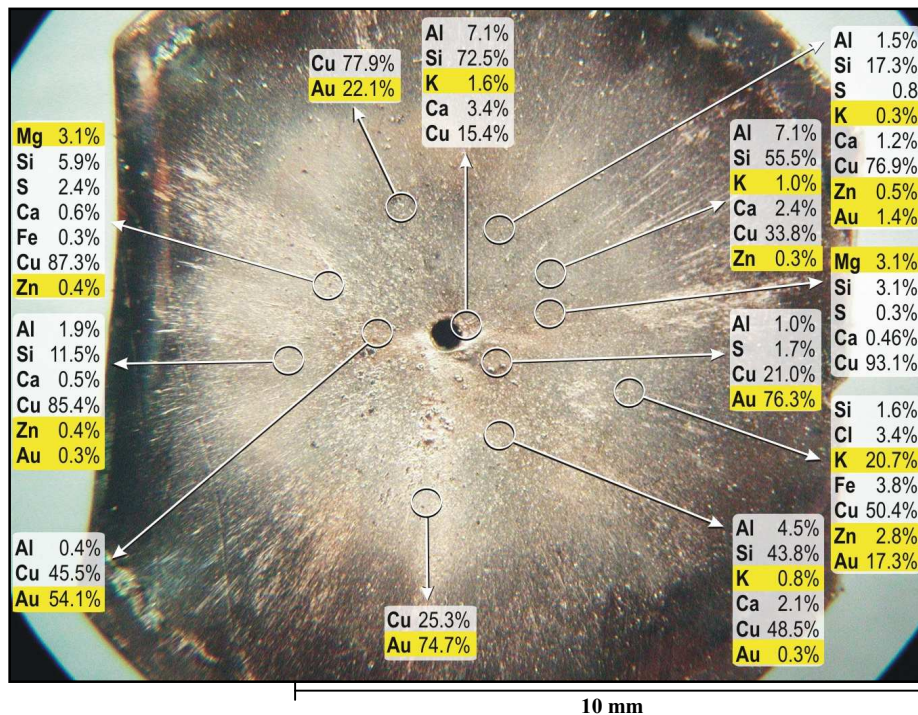


Fig. 20. Accumulating screen after experiment No. 2107.
 The material of the accumulating screen is copper (Cu 99.99%).
 The method of investigation is X-ray electron probe microanalysis.
 (Element detection range – from Na to U).

The amount of the atoms precipitated on the accumulating screen in the process of a target collapse was thoroughly evaluated with local and integral analytical methods.

Local analysis of the accumulating screens by X-ray electron probe microanalysis

The local analysis was performed with X-ray electron probe microanalyzer REMMA-102 (Ukraine). Characteristic X-ray emission was excited by the electron 35-keV, 0.1-nA beam. The sample under study was the copper accumulating screen (Cu 99.99 mass. %). The scheme of analysis is presented in Fig. 21.

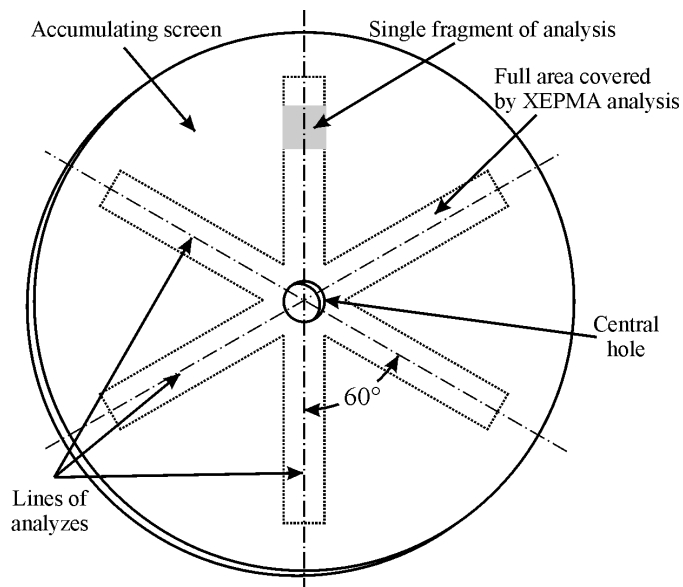


Fig. 21. Scheme of the XEPMA analysis.

Average amount of synthesized atoms precipitated on the accumulating screen No. 5094 was estimated from composition analyses of 417 microparticles and 113 fragments on its surface. The result of extrapolation gives the value of 1.2×10^{18} synthesized atoms.

The drawback of the local method is that this estimation was obtained as a result of extrapolation rather than a result of fully direct measurement. Moreover, we can't exclude the probability that the atoms we consider as synthesized appeared on the surface as a result of redistribution of admixtures in the volume of accumulating screen.

Integral analysis of the accumulating screens by glow-discharge mass-spectrometry

For the integral analysis we used high-resolution glow-discharge mass-spectrometer VG-9000 (VG Elemental, UK) with mass detection range 1...250 a.m.u. and mass resolution $M/\Delta M = 7000...9000$. This instrument recently has become generally accepted for complete and accurate element characterization of materials, especially suited for trace and ultra-trace analyzes. The task was to determine and to compare the composition of the accumulating screen before and after the experiment.

Then the number of synthesized atoms was calculated as a difference between these values.

It is worth to be mentioned that this method has some peculiarities:

- ◆ the method is destructive one;
- ◆ the process of elemental composition registration of the investigated sample is going on sequentially.

Therefore the analyzed sample must have homogeneous in depth composition. It is obvious that the frontal analysis of the accumulating screen surface would give the wrong result, because the layer of precipitated nucleosynthesis products is very thin. So, to get a rather homogeneous sample for integral analysis an assembly from a number of accumulating screens, which were used in identical experiments, was prepared (Fig. 22).

The cross-section of such assembly subject to analysis with VG-9000 is 5 mm in diameter contains not less than 10 cross-sections of screens. Such procedure in essence is a direct measurement of the accumulating screen elemental composition and provides a high averaging level of the measurable value.

Data processing of the results of numerous HRGD-MS measurements of the assemblies from Cu (99.99 mass. %) accumulating screens after experiments with Al (99.94 mass. %) targets gave the number of synthesized atoms precipitated on the single screen after the target explosion equal to 2.29×10^{18} (0.23 mg). The same measurements but made after experiments with Ag (99.95 mass. %) targets gave the value of 3.33×10^{18} (0.30 mg). It is clear that these values well adjust with the data of local analysis and those obtained in experiments on ^{60}Co deactivation.

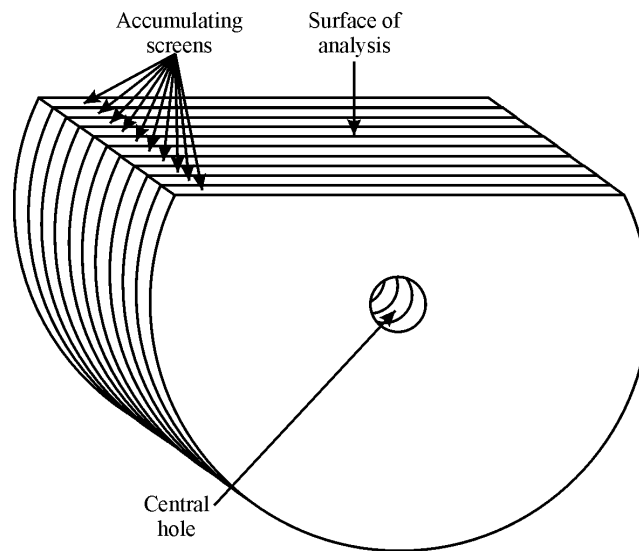


Fig. 22. Sample for integral HRGD-MS analysis.

Analysis of the isotope composition of inert gases in a residual atmosphere of the vacuum chamber

The main task was to measure the argon (Ar) isotopic composition in the probes from reaction vacuum chamber where the experiments on high-energy compression of solid targets were carried out.

The results of the isotopic composition measurements have shown that probes contained isotopes in anomalous ratios $^{40}\text{Ar}/^{36}\text{Ar}$ (Fig. 23).

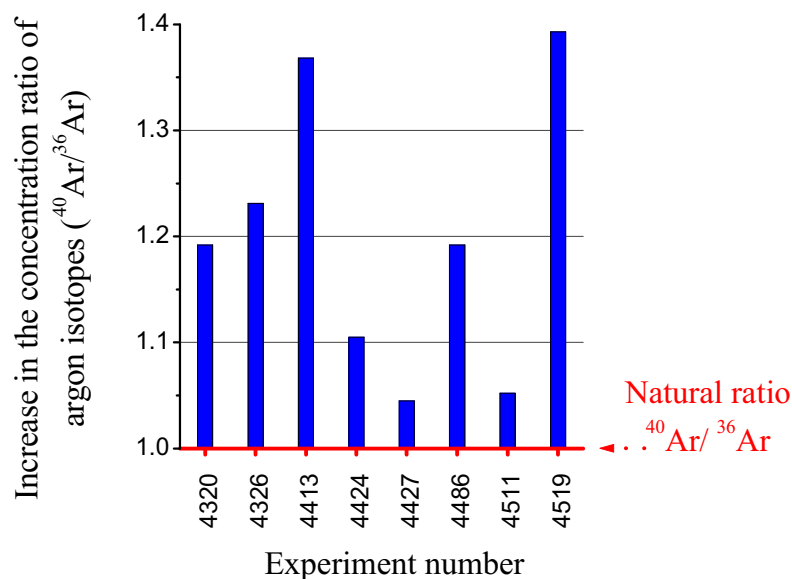


Fig. 23. Increase in the ratio $^{40}\text{Ar}/^{36}\text{Ar}$ in vacuum chamber in comparison to atmospheric. Method of investigation is mass-spectrometry (MI-1201IG).

Analysis of the isotope composition of accumulating screens

The analyses of the isotope composition were performed by the methods of mass spectrometry. As was found, the majority of analyzed microprobes of a substance of accumulating screens had the isotope composition different from the natural one. Below, we present the examples of the isotope composition for some elements (Figs. 24, 25).

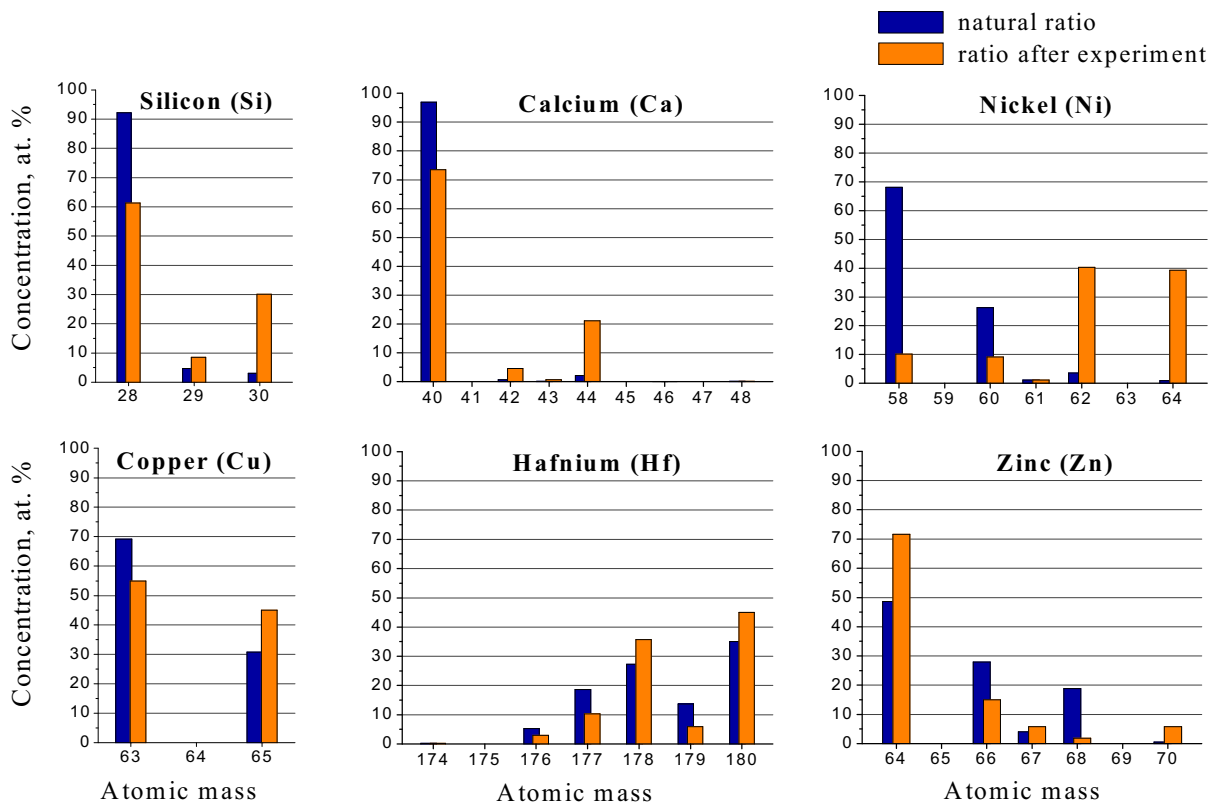


Fig. 24. Examples of anomalous isotopic ratios of some chemical elements detected on the surface of the accumulating screens.

The method of investigation is secondary ion mass-spectrometry (IMS-4f).

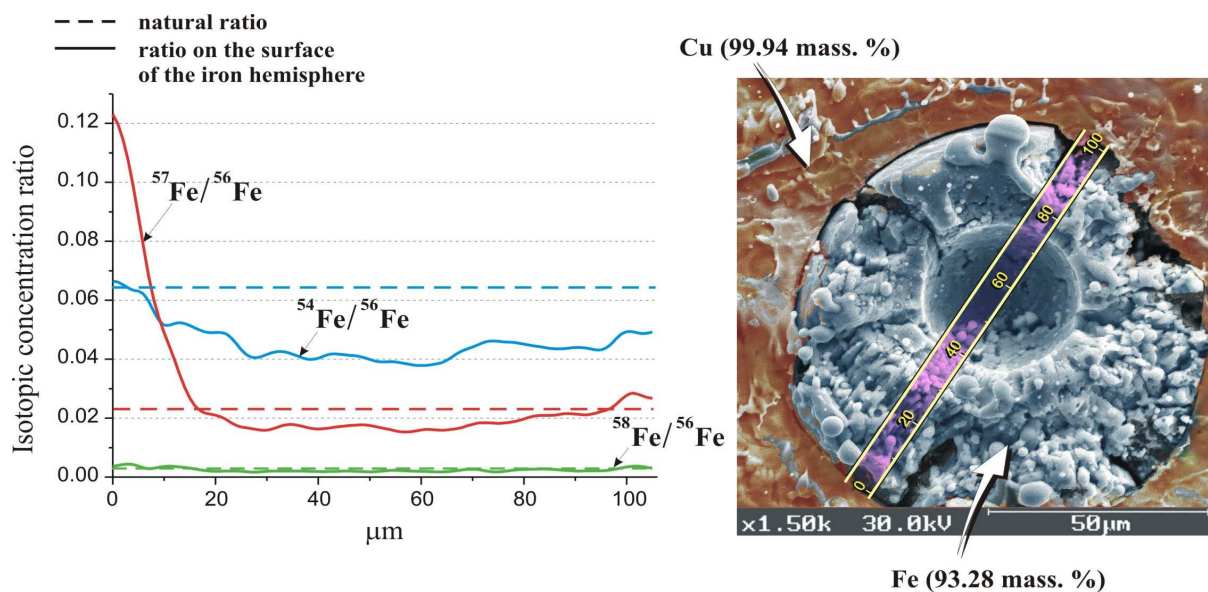


Fig. 25. Anomalous isotopic ratio of iron on the surface of hollow iron (Fe) hemisphere discovered on the surface of the copper accumulating screen after the experiment with the copper target.

The method of investigation is secondary ion mass-spectrometry (IMS-4f).

Distributions of various chemical elements over depth in accumulating screens

During the study of the element and isotope compositions of near-surface layers of accumulating screens, the nonuniform distributions of the concentrations of chemical elements over depth were discovered. A peculiarity of these distributions consists in that the impurity elements with different atomic masses and charges form a layer with maximum concentration at the same depth. Its distance from the surface is different in different experiments.

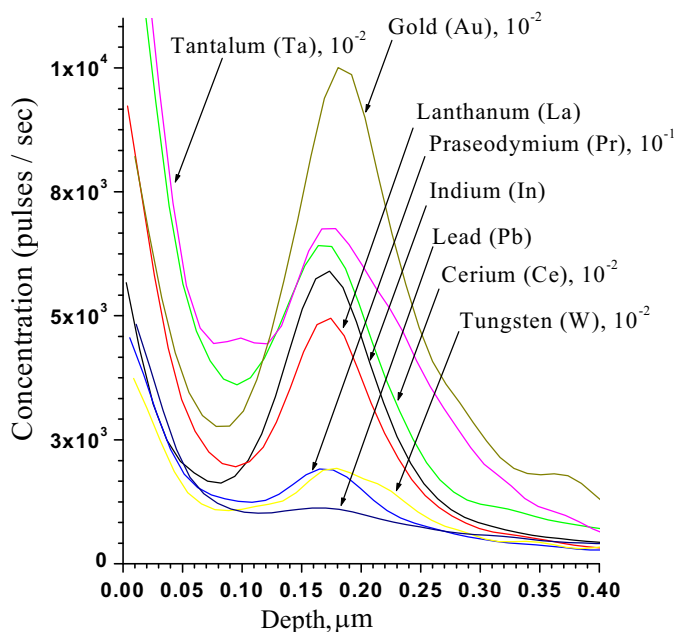


Fig. 26. Concentration maximums in the screen after experiment No. 2670. The material of a target and an accumulating screen is copper (Cu 99.99%).

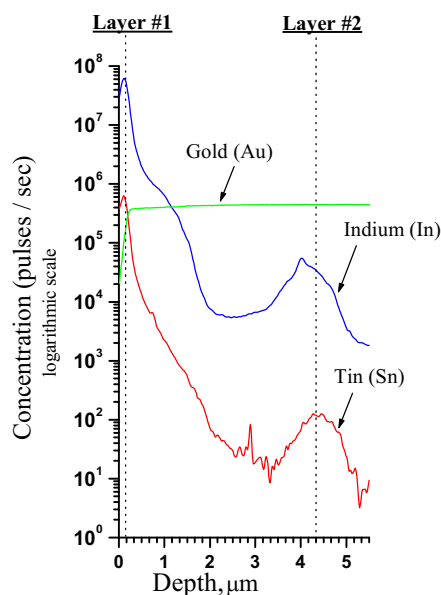


Fig. 27. Concentration maximums in the screen after experiment No. 1855. The material of a target and an accumulating screen is gold (Au 99.99%).

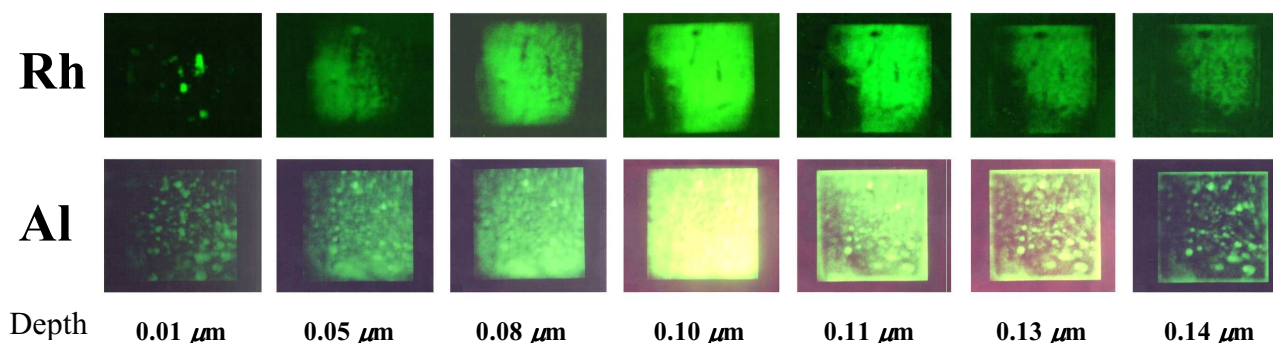


Fig. 28. Distribution of the concentration of rhodium (Rh) and aluminum (Al) over depth. The image is formed by secondary ions. The concentration is proportional to the image intensity. The image is 0.5×0.5 mm. The material of a target is lead (Pb 99.91%), and the material of an accumulating screen is copper (Cu 99.99%). Experiment No. 2828.

Decrease in the γ -activity of radioactive isotope of cobalt ^{60}Co

The experiments were carried out in a cylindrical caprolone chamber schematically shown in the Fig. 29. The envelope with a capsule was positioned at the chamber center. Before the experiment, the measurement of radioactivity was performed at two different distances from the chamber center to the detector surface (75 and 755 mm depending on the target radioactivity). At each distance, we measured the radioactivity of the chamber with detectors being in 4 positions, with the turn by 90° from each position to the next one. As the initial radioactivity level for a given distance, we took the arithmetic average over 4 measurements. The chamber interior was evacuated together with the whole setup, with the valve open. Several seconds before the experiment started, we closed the valve and sealed the chamber. After the high-energy impact affected the target, the chamber remained vacuumized until the completion of all measurements. After the experiment, we measured the level of radioactivity with the detectors at the same distances and positions as before the experiment.

Activity of the targets was detected by Ge(Li)-detectors with volume 160 cm^3 and resolution 2.2 keV on γ -lines 1173.2 and 1332.5 keV.

After the explosion, the target remnants were sprayed over the interior surface of the chamber. Therefore, the validity of calculation method was experimentally tested by intentionally spreading the activity over the chamber's internal surface.

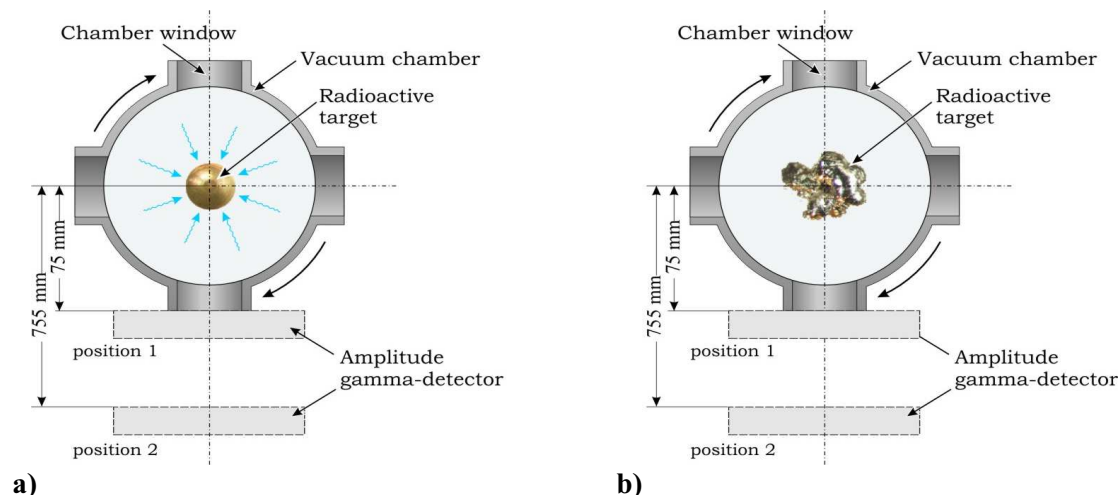


Fig. 29. Scheme of the experiment on the gamma-activity decrease that depicts the initial state (a) and the state after the driver action (b).

Table 6. Decrease in the γ -activity of ^{60}Co after the experiment

Number of sample	Decrease in the γ -activity, %	Number of sample	Decrease in the γ -activity, %	Number of sample	Decrease in the γ -activity, %
2397	47.6	2479	2.2	2588	46.5
2398	10.7	2481	22.8	2600	33.3
2425	21.6	2534	29.5	2769	28.9
2426	17.0	2558	22.9	2770	36.4

Extraordinary results

The analyses of the results of experiments performed with the use of heavy targets [platinum (Pt), lead (Pb), and bismuth (Bi)] showed that the surfaces of accumulating screens contain the long-lived isotopes of heavy chemical elements with atomic numbers close to the boundary and beyond the limits of the well-known part of the Periodic Table of elements.

Registration of the unidentifiable atomic masses with the mass number >220 a.m.u in near-surface layers of accumulating screens by the secondary ion mass-spectrometry

Characteristics of the unidentifiable masses are the following:

- Masses were absent in the survey spectra of the reference materials;
- Distribution of the unidentifiable masses did not coincide with distribution of other chemical elements on the analyzed surface;
- The higher was the shift voltage in the Offset mode the higher was the intensity of the unidentifiable peaks in comparison to the peaks of clusters of other chemical elements detected on the analyzed surface.

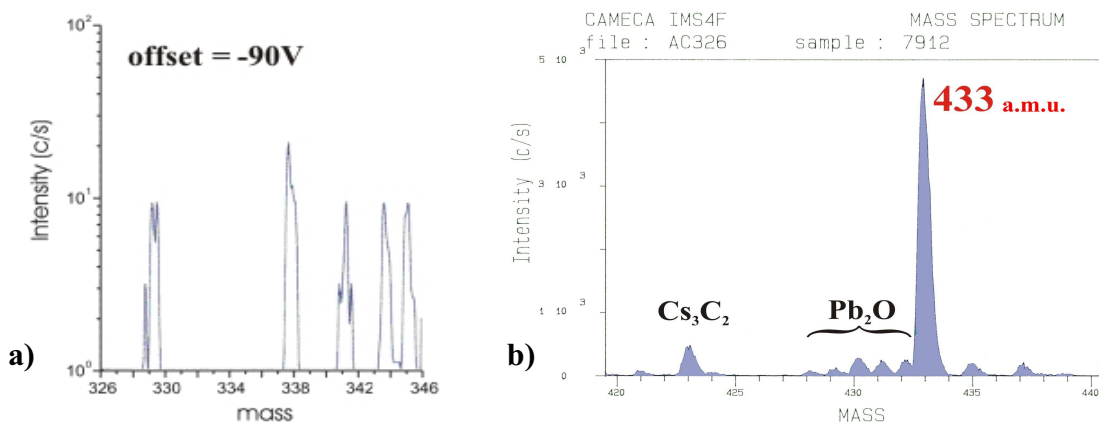


Fig. 30. Secondary ion mass spectrometry (IMS-4f, analyzed mass range — up to 500). Unidentifiable masses of chemical elements in the range of atomic masses from 326 to 346 (a), and near 433 (b).

Registration of the scattering centers, corresponding to the mass numbers > 200 a.m.u., in the energy spectra of scattered α -particles and nitrogen ions (^{14}N)

Taking into account the peculiarities of the targets containing the products of nucleosynthesis the time-of-flight technique was developed and implemented to identify heavy ions by Rutherford backscattering of α -particles and ^{14}N ions on nuclei composing the near-surface layers of the targets.

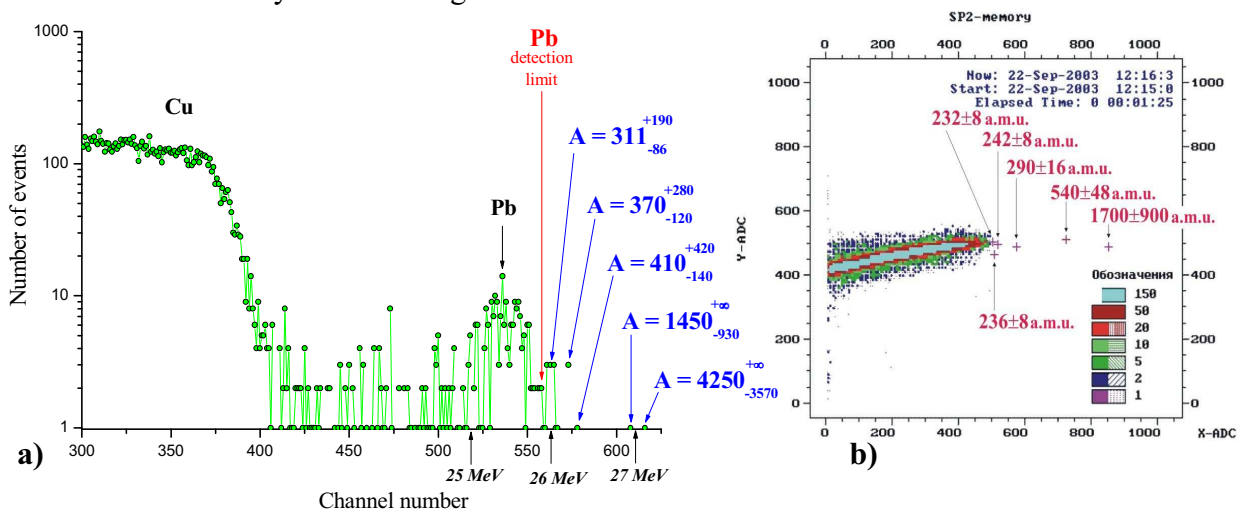


Fig. 31. Rutherford backscattering of α -particles at an angle of 135° accelerated up to an energy of 27.6 MeV (a) and nitrogen ions (^{14}N) at an angle of 150° with initial energy of 8.7 MeV (b).

Registration of the unidentifiable peaks of characteristic X-ray and Auger emission in the elemental composition analysis of the accumulating screens surface

On the surface of accumulating screens the unidentifiable Auger-peaks with energies of 172, 527, 1096, 94, and 560 eV and the doublet of peaks with energies of 130 and 115 eV were registered (Fig. 32). They, on the one hand, are not related to the peaks of the known chemical elements in existing catalogues and, on the other hand, in our opinion cannot be considered as artifacts.

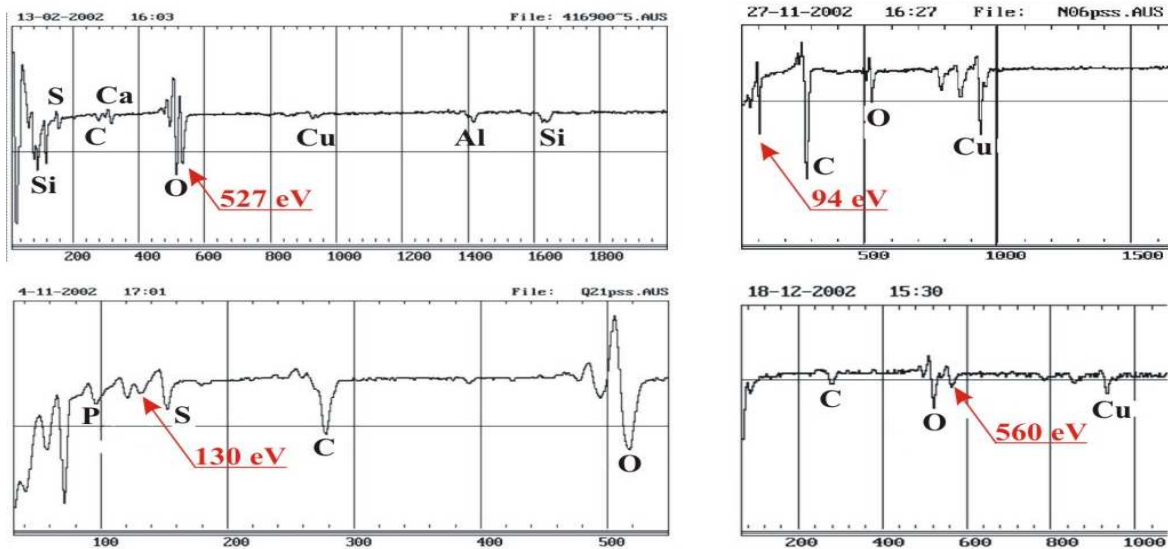


Fig. 32. Auger-spectroscopy (JAMP-10S, element detection range – all but H and He). Unidentifiable Auger-peaks of 527, 94, 560, and 130 eV.

On the surface of the accumulating screen of the sample No. 8545 the unidentifiable characteristic X-ray radiation peaks of low intensity with the energies of 23.582 and 28.943 keV (Fig. 33). These peaks do not relate to the artifact of analysis known as the peak of “sum” appearing as a result of simultaneous detection of two gamma quanta with different energy. The amplitude of the registered low intensity peaks was more than three times higher than the root-mean-square fluctuation of the X-ray background that evidences the high reliability of the registered peaks.

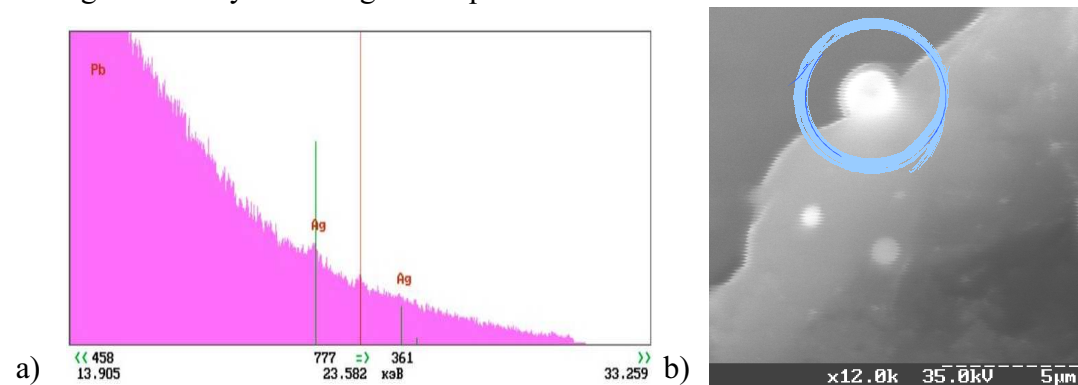


Fig. 33. X-ray spectrum microanalysis (REMMA 102, element detection range — all starting from B). Unidentifiable peak of X-ray emission on the sample No. 8545 with energy 23.582 keV, estimated nucleus charge is 118-119 (a); location of the unidentifiable peak (b).

Study of the samples by independent laboratories

Extracts from the official conclusion of the concern “Luch”, Russia, concerning the analyzed objects given by the firm “Proton-21” for mass spectrometric analysis on a device “Finnigan” MAT-262:

The analysis of the isotope compositions of the samples showed that all samples except for the control one reveal the considerable deviations from the natural isotope ratios for many elements: Si, K, Ca, Ti, Cr, Fe, Zn, Zr, Ba, and others. These deviations are large and lie far beyond the limits of errors.

In addition, the mass spectra reveal the masses equal to 253, 264, 394, 395, 433, and 434 which do not yield to any interpretation and identification, i.e., they are absent among all the known isotope combinations given in the typical catalogs.

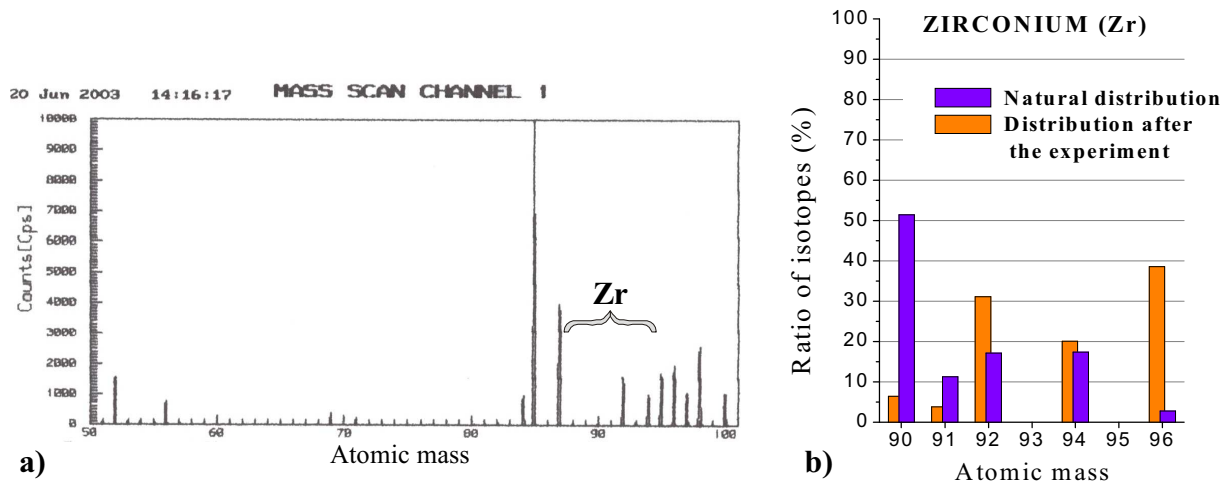


Fig. 34. Thermal-ionization mass spectrometry (MAT-262, mass detection range – up to 470). The violation of the isotope composition of zirconium (Zr): mass spectrum (a), comparative histogram (b).

Extracts from the official conclusion of MICRO PHOTONICS (Surface Test), REPORT SIMS-030623 for United Metals LLC (USA):

...The presence of heavy ions with masses equal to 221, 222, 223, 224, 225, 226, 232, 233, 235, 236, 239, 240, 241, 243, 247, 257, 259, 263, 265, and 266 is found.

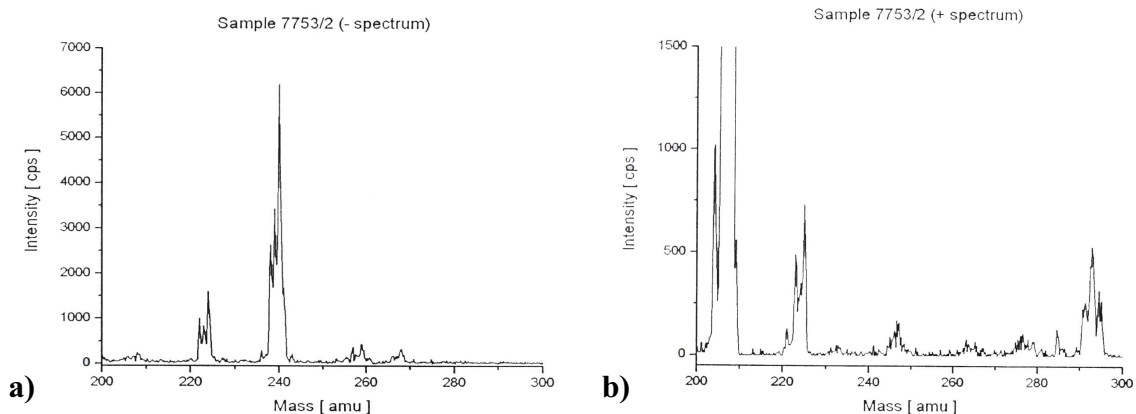


Fig. 35. Secondary-ion mass spectrometry (SIMS, analyzed mass range – up to 300). Nonidentified atomic masses. The mass spectrum is given for negative ions (a) and positive ions (b).

Results and conclusions

The results of the experiments are the following:

- The effectiveness of nuclear transformations depends on the initial target material composition and is equal approximately to 10^{15} – 10^{16} synthesized atoms per 1 J of input energy.
- The levels of α -, β - and γ -emissions of the products of nuclear transformations do not exceed the background ones. Multiple γ - and β - spectrometry tests revealed that the relative concentration of radioactive nuclei of all synthesized isotopes does not exceed $\eta \approx 10^{-8} \dots 10^{-12}$.
- Decrease in the γ -activity of the targets with radioactive isotopes is equal to the transmutation of 2.5×10^{18} nuclei of the target focal zone (focus of the driver action) for the driver energy about 1 kJ. The absolute value of the activity decrease depends on concentration of radioactive nuclei in the target focal zone.
- Formation, evolution, and disintegration of electron-nuclear collapse are accompanied with point X-ray radiation with temperature $T \approx 35$ keV and duration about 10^{-8} s.
- Kinetic energy of corpuscular component of the plasma bunch (ions and electrons together) is about 1 kJ.
- The long-living isotopes of superheavy chemical elements are found in the products of the laboratory nucleosynthesis.

These results lead to the following conclusions:

- The impact-induced compression could initiate the process of nuclear transformation of a initial target material in the collapse zone, which is confirmed by:
 1. increase by orders in the concentrations of chemical elements being admixtures in a target;
 2. detection of chemical elements (including rare ones) which were not found by highly sensitive analysis (down to 10^{-10} %) in the starting materials of the targets, accumulating screens, as well as in residual gases of the vacuum chamber;
 3. considerable violation of the well-known isotope abundances of chemical elements including those of inert gases formed in the working chamber volume;
 4. decrease in the γ -activity of the radioactive isotopes of cobalt (Co), silver (Ag), and zinc (Zn).
- The nuclear reactions initiated in a target are collective and multiparticle. It is proved by the presence of a considerable number of nuclei ($> 10^{16}$) with the mass two and more times heavier than that of the starting target material in the products of nucleosynthesis.
- The developed driver demonstrates high reproducibility of the compressed substance conditions required for initiation of the collective multiparticle reactions in a macrovolume of a substance.
- Experimental data prove that coherent pulse driver is able to initiate the avalanche-like process of energy concentration in a cold solid substance that results in the energy-efficient nuclear reactions.